International Journal of Heat and Mass Transfer 223 (2024) 125262

Contents lists available at ScienceDirect

International Journal of Heat and Mass Transfer

journal homepage: www.elsevier.com/locate/ijhmt

Tunable self-extinguishing of dripping fire mediated by impacted substrates

Xujun Fan [a,b], Fangye Lin [b,*], Stéphane Dorbolo [c,*], Wei Wang [d], Jun Zou [a,*]

[a] State Key Laboratory of Fluid Power and Mechatronic Systems, Zhejiang University, Hangzhou 310027, China
[b] Ningbo Innovation Center, Zhejiang University, Ningbo 315100, China
[c] Département de Physique, FNRS-CESAM-GRASP, Université de Liège, B-4000, Belgium
[d] Hangzhou City University, Hangzhou 310015, China

ARTICLE INFO

Keywords:
Dripping fire
Fire extinguishing
Burning droplet
Droplet evaporation

ABSTRACT

Dripping fire, caused by flammable liquids falling onto solid surfaces, presents a significant challenge for fire hazard management due to its concealed and unpredictable nature. In this study, we investigate the evaporation and burning characteristics of dripping fire and ascertain that self-extinguishment can occur under specific drip masses and frequencies owing to heat transfer from the heated substrate to the droplet and thermocapillary motion of burning droplets. By controlling these drip parameters, we observe three distinct burning regimes: non-extinguishing, self-extinguishing, and non-igniting; furthermore, we confirm that their critical drip masses and frequencies follow a power function with an exponent of 3/2. We develop an evaporation model to predict the occurrence of the self-extinguishing regime, which aligns well with experimental results. Additionally, by designing substrates with diverse surface structures and thermal properties to manipulate evaporation dynamics and motion behavior of burning droplets, it is possible to significantly reduce the burning duration of dripping fires from over 120 s to under 20 s. Overall, this finding offers a novel approach to mitigating fire hazards related to flammable drips in various settings such as buildings and industrial environments.

1. Introduction

Fire has always played a significant role in the history of human civilization, yet it also inflicts substantial casualties and economic losses on society every year. A common phenomenon in fires is the continuous dripping of flammable liquids, such as copaiba oil flowing from injured tree trunks [1], liquid wax falling from tilted burning candles, molten thermoplastic materials dripping from building facades [2], and fuel liquids leaking from storage tanks [3]. These inconspicuous millimeter/centimeter-sized flammable drips, known as dripping fire when ignited, are often a significant cause of serious fires [4–6].

In previous studies, the investigation of dripping fire mainly focused on the ignition, burning, and dripping processes, yielding valuable insights into fire characteristics and hazard analysis. For example, Wang et al. [7] examined the impact of ignition location on the combustion behavior of molten polymer drips. They found that the initial ignition location significantly influenced fire parameters such as heat release rate, released heat, smoke temperature, CO concentration, and extinguishing coefficient, leading to different fire spread types. Sun et al. [8] conducted experiments on polyethylene drips igniting thin paper, similar to classical pilot ignition of thin fuels. They observed that the ability of burning drips to ignite paper decreased with increasing paper thickness, with ignition time inversely proportional to drip mass and frequency squared. Xie et al. [9] investigated the dripping-burning and flow behavior of thermoplastic material drips (polystyrene (PS), polyethylene (PE), and polypropylene (PP)). They found that the drip frequency and flame spread velocities of PP and PE were higher than that of PS, while the pool fire burning rate of PP and PE was lower. Considering heating, melting, drip frequency, and flow combustion behavior, the researchers concluded that the flow fire hazard of PE and PP was significantly higher than that of PS. Kim et al. [10] predicted the drip size and time of molten polymer droplets in dripping fires through numerical simulations. Their study revealed a linear correlation between the total heat flux at the melting front and its length. Using force balance equations, they estimated drip size and time, which correlated linearly with modified inverse Bond number and a combination of capillary number and modified Bond number. He et al. [11] experimentally investigated the dripping behavior of melting insulation in copper wire under overload current. They found that dripping behavior correlated with strong currents, and drip frequency was proportional to the square of the current. Additionally, dripping behavior influenced flame propagation along energized wires, resulting in variations in flame width,

* Corresponding authors.
E-mail addresses: linfy@zju.edu.cn (F. Lin), s.dorbolo@uliege.be (S. Dorbolo), junzou@zju.edu.cn (J. Zou).

https://doi.org/10.1016/j.ijheatmasstransfer.2024.125262
Received 27 November 2023; Received in revised form 24 January 2024; Accepted 29 January 2024
Available online 4 February 2024

height, and propagation velocity. In summary, these studies primarily contribute to an understanding of the combustion characteristics and fire hazards associated with dripping fire.

In recent years, there has been growing interest in controlling the fire hazards associated with drip materials like polymers and flammable fuels due to their widespread application field. Researchers have explored various approaches to address this issue. For instance, Carosio et al. [12] investigated the effect of ionic strength of polyhedral oligomeric silsesquioxane and sodium montmorillonite coatings assembled through layer-by-layer on the melt dripping of polyester fabrics. These coatings effectively suppressed drip formation, slowed down flame spread, and reduced the combustion intensity of the fabrics. Guan et al. [13] developed a fire-resistant triboelectric nanogenerator (TENG) based on fully aromatic liquid crystal poly (aryl ether ester) (LCP_{AEE}). The TENG, utilizing LCP_{AEE} as a high-rigidity main chain material, exhibited excellent resistance to drip formation, high temperatures, and fire. Wu et al. [14] enhanced the flame retardancy and mechanical properties of epoxy resin by synthesizing a phosphorus-containing organic-inorganic hybrid flame retardant (APOP). Additionally, researchers have explored the use of acoustic waves to extinguish fast-moving dripping flames. Xiong et al. [15] found that the effectiveness of acoustic wave extinguishment decreased with increasing dripping velocity. They [16] also discovered the use of acoustic waves to extinguish propane flames and found that the frequency and sound pressure of the acoustic source had a significant effect on the flame. Lower-frequency acoustic sources produced larger membrane vibrations and flame flicker displacements, promoting flame extinction. These approaches offer potential strategies for mitigating the fire hazards associated with dripping fires. However, their practical application is limited by the complexity of the required working conditions. In real fire scenarios, when the flammable liquids drop on a solid surface, preventing the accumulation of flammable drips and reducing their burning time and fire spread are crucial for controlling fire hazards. Notably, there is limited research on how burning drips interact with solid surfaces and how solid surface properties can be utilized to control fires.

In this work, we propose a hazard control method for dripping fires based on the design of the surface structure and thermal properties of the solid substrate. We investigate the burning and evaporation behaviors of continuous fuel drips on the substrate surface, and identify three burning regimes: non-extinguishing, self-extinguishing, and non-igniting, depending on the drip mass and frequency. We find that the burning regime and duration of a dripping fire are influenced by the thermocapillary motion of the droplet and the heat transfer from the heated substrate to the droplet. Based on these insights, we design a range of substrates that modify the motion and evaporation behavior of burning drips, resulting in a significant reduction in burning time from over 120 s to under 20 s. These findings offer a straightforward and effective approach for controlling the hazards of dripping fire.

2. Materials and methods

2.1. Preparation of materials

Ethanol (99.8 %, [vol/vol]), methanol (99.5 %, [vol/vol]), and isooctane (99.0 %, [vol/vol]) were purchased from Sinopharm Chemical Reagents Co., LTD. The physicochemical properties of these liquids are provided in Table S1. Silicon substrates without surface microtextures were processed by Zhejiang Jingxin Technology Co., LTD, while silicon substrates with surface microtextures were fabricated by Suzhou Yuanwei Chip Technology Co., LTD. Sapphire substrates were manufactured by Suzhou Hengjia Crystal Material Co., LTD, and the quartz substrate was fabricated by Lianyungang Aokai Quartz Co., LTD. Tables S2 and S3 display the physical parameters of all substrates. The surface microtextures on the silicon substrates were created using photolithography and ion etching processes. Firstly, a uniform layer of positive photoresist AZ4620 (Shipley, US) was applied to the cleaned silicon substrate. The coated silicon substrate was then dried and cured at 100 °C for 2 min. Subsequently, double-sided alignment and contact exposure were performed using the MA6 UV MASK ALIGNER (SUSS MicroTec, Germany) for 30 s. The exposed silicon was soaked in a Tetramethylammonium hydroxide (TMAH) solution (25 % TMAH: deionized water = 1:8) for 1 min. The silicon substrate was then rinsed with deionized water and dried at 100 °C for 5 min followed by 110 °C for 7 min. After the treatment, the exposed silicon was etched using a MULTIPLEX ASE-HRM ICP ETCHER (Surface Technology Systems plc, UK) with a radio-frequency power of 200 W and an etching rate of 10 μm/min. Following etching, any excess photoresist was removed with acetone, and the microtextured silicon substrate was rinsed with ethanol and deionized water before being dried. The surface microtopography of all substrates was examined using Laser Scanning Confocal Microscopy (LSCM) (see Fig. 1).

2.2. Dripping fire experiments

The experimental setup can be seen in Fig. 2a. A syringe pump was used to push out continuous flammable drips with a constant mass and frequency from the needle tip. The starting droplets (3 drops by default) would reach the substrate surface and form a kindling liquid film, which was then ignited. The subsequent evaporation and burning processes of the continuous drips on the substrate were recorded using camera 1 (a high-speed camera, Phantom v2512) at a frame rate of 1000 fps and camera 2 (a digital camera, Sony FDR-AX60) at a frame rate of 25 fps, respectively, under different lighting conditions. It is important to note that two thermal baffles were employed to ensure their minimal interference with the experimental results. Firstly, a thermal baffle with a small round hole (approximately 1 cm in diameter) was placed between the needle and the impacted substrate to prevent wide-ranging heat airflow (fire plume) from disrupting the continuous liquid dripping process. Secondly, the impacted substrate was positioned on another thermal baffle (shown in Fig. 2a) to reduce conductive heat loss from the bottom of the substrate. The ambient temperature during the experiment was 20 ± 1 °C. The impact velocity v_0, mass m_0, and frequency f of the ethanol drip varied within the range of 2.12 ~ 3.06 m/s, 1.7 ~ 13.8 mg, and 0.14 ~ 6.67 Hz, respectively.

2.3. Parameters measurement

The mass m_0 (or diameter D_0) and Weber number We (or velocity v_0) of the drip before impact, as well as the frequency f and solid-liquid contact area S_c during impact, are identified and calculated from experimental images taken by the high-speed camera. The uncertainties for length, mass, and time are 0.05 mm/pixel, 0.1 mg, and 0.001 s, respectively. The substrate temperature T_s was captured using the temperature acquisition system (DAM-4501, Xunyan Electronics Co. LTD, China) with a response time of 500 ms. Two superfine surface K-type thermocouples (0.05 mm in diameter), positioned at the center and the edge, were used and fixed at the bottom of the substrate (1 mm thick). Since the substrate surface is square or circular (i.e. 35 mm in length or 39.5 mm in diameter with the same surface area), the temperature recorded at these two points can represent the overall substrate temperature (temperature differences in the direction of thickness are ignored). The experimental analysis and calculation of substrate temperature and the error bar (or error band) were based on the temperature readings from the two measuring points with an uncertainty of ± 0.1 °C. The burning time (or duration) t_b of the fire was obtained by recording the time interval from the ignition of the kindling liquid film to the complete extinguishing of the fire using the digital camera, with an uncertainty of ± 0.1 s. The burning time for the non-extinguishing phenomenon was recorded for more than 10 min. The flame size, including the height H_f and volume V_f, was calculated using a gray-threshold method [17,18] based on side-view flame images (see Fig. 2b). Firstly, the entire outline of the flame in each frame was

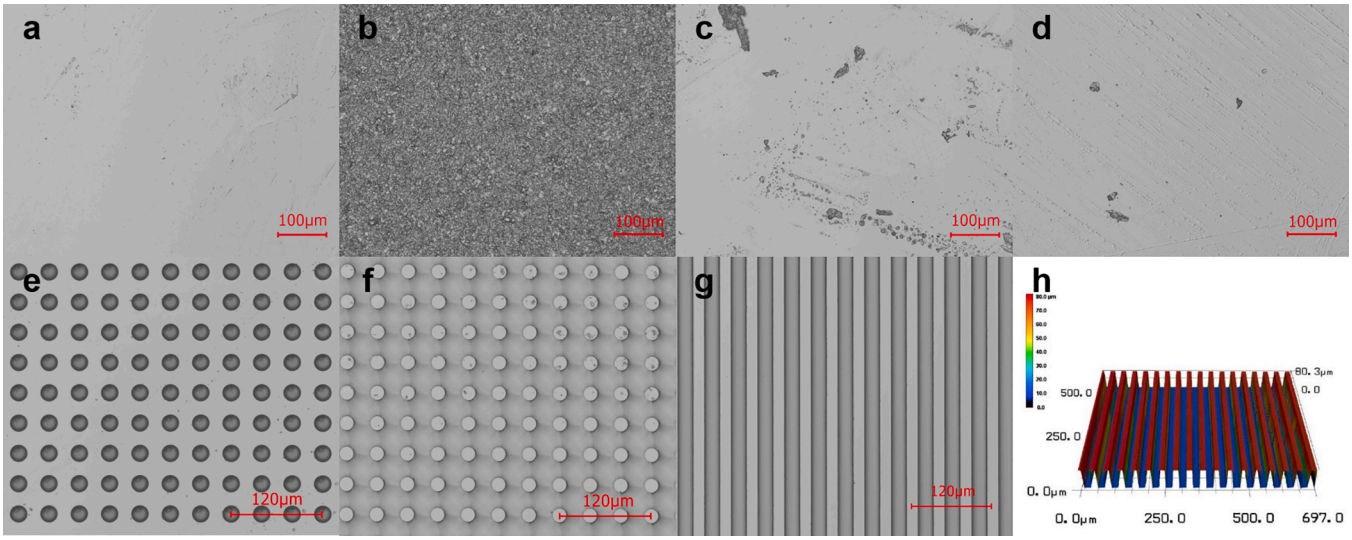

Fig. 1. Surface microtopography of different substrate surfaces under Laser Scanning Confocal Microscopy (LSCM). (a) Smooth silicon. Rough surfaces: (b) Silicon, (c) Sapphire, (d) Quartz. Microtextured silicon surfaces: (e) Micropore, (f) Micropillar, (g) Microgroove. (h) The corresponding three-dimensional morphology of the microgrooved surface in (g).

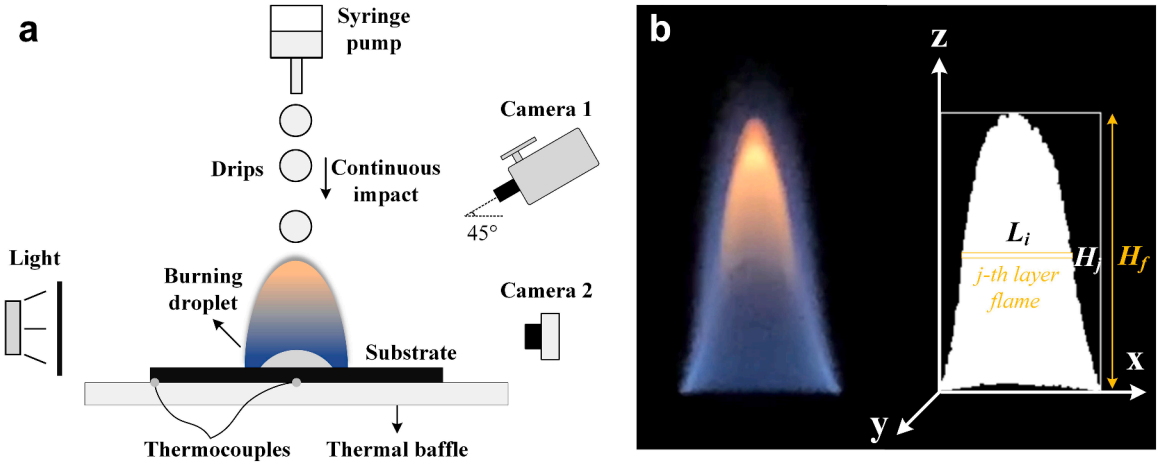

Fig. 2. (a) Experimental setup for capturing the evaporation and burning behaviors of continuous droplets on the impacted substrate. (b) Binary flame image recognition by gray threshold method.

identified by setting a grayscale threshold, which allowed for the determination of the flame boundary and maximum height. Secondly, utilizing the infinitesimal method, the flame was divided into n_1 layers from bottom to top (further divided into n_2 micro-cylindrical flames from left to right if there are multiple discontinuous flames). The equivalent diameter of the j-th flame layer can be expressed as $D_j = (\sum_{i=1}^{n_2} L_i^2)^{1/2}$, where i and L_i represent the i-th micro-cylinder and the horizontal diameter of the i-th micro-cylinder in the j-th layer flame, respectively. Then, the volume of the j-th layer flame can be indicated as $V_j = \frac{\pi}{4} D_j^2 H_j$, where H_j is the height of the j-th layer flame. Consequently, the total volume of the flame can be expressed as $V_f = \sum_{j=1}^{n_1} V_j$, which yields $V_f = \frac{1}{4}\pi \sum_{j=1}^{n_1} (\int_0^{H_j} \sum_{i=0}^{n_2} L_i^2 dz)$. Finally, the transient sizes of the flame were obtained by compiling the computational code.

3. Results and discussion

3.1. Self-extinguishing phenomenon

Let us start with a case study in Fig. 3: ethanol drips with a mass m_0 of 2.9 mg were continuously impacting onto a smooth silicon substrate (surface roughness $Ra < 0.1$ μm) at a constant Weber number We ($We = \rho D_0 v_0^2 / \sigma$, where ρ, D_0, v_0, and σ are the density, diameter, impact velocity, and surface tension of the drip before contact with the substrate) and frequency f. We recorded the burning and evaporation processes separately in Fig. 3a and b and measured the key parameters such as the flame height H_f and volume V_f, the contact area S_c of the burning droplet on the substrate before the arrival of the next drip, and the average temperature T_s of the substrate as a function of time t in Fig. 3c. The results show that the dripping fire undergoes three distinct burning stages before self-extinguishing (see Movie S1): the ignition and burning of the liquid film (stage 1, $t_1 \sim t_2$), steady-state burning of sessile droplets (stage 2, $t_2 \sim t_3$), and unsteady burning of moving droplets (stage 3, $t_3 \sim t_4$).

Stage 1 is characterized by a rapidly varying flame size due to the large S_c ($t_1 \sim t_2$ in Fig. 3c) and the visible splash caused by the drip impinging on the liquid film (at 0.017 s in Movie S1). This is the initial development of the dripping fire that forms after being ignited ($t_1 = 0$ s), with a light blue flame indicating full combustion.

Stage 2 is distinguished by the burning droplet being relatively fixed in location. The flame size periodically oscillates as each new drip spreads on the substrate ($t_2 \sim t_3$ in Fig. 3c). Note, however, that the

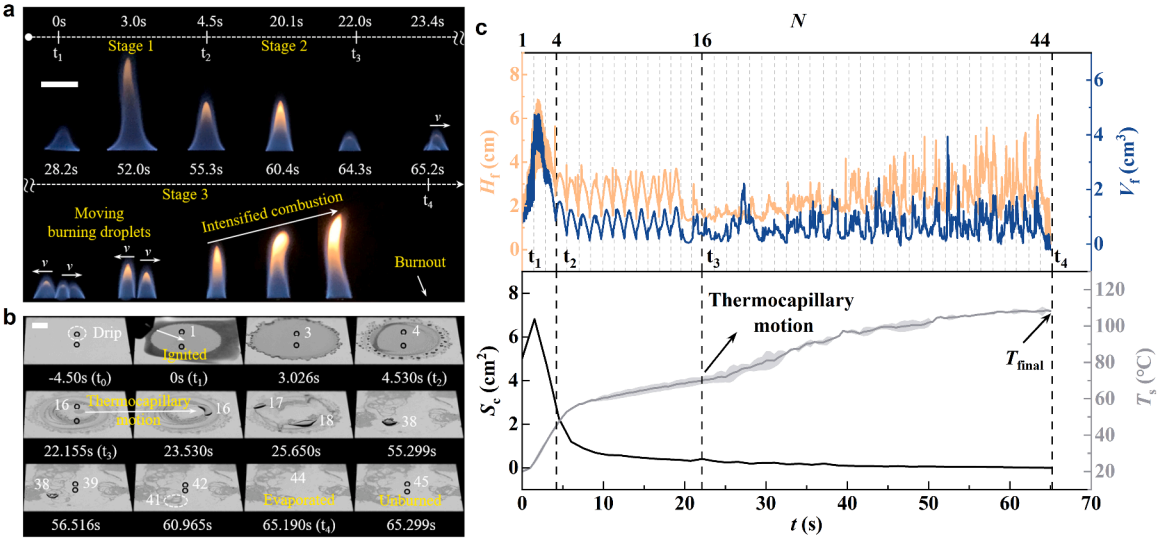

Fig. 3. Self-extinguishing phenomenon of an ethanol dripping fire on a smooth silicon substrate ($m_0 = 2.9$ mg, $We = 305$, $f = 0.67$ Hz). (a and b) The burning and evaporation processes of continuous ethanol drips before fire self-extinguishing. (c) Flame size (height H_f and volume V_f), solid-liquid contact area S_c, and substrate temperature T_s as a function of time t and drip number N before fire self-extinguishing. Each thin dashed line represents one drip and the gray shaded band around T_s indicates the uneven distribution of substrate temperature. In (a-c), t_0 is the start time of the dripping behavior, t_1, t_2 and t_3 are the start times of each burning stage, and t_4 is the end time of the fire. The numbers (1 ~ 45) next to the drips in (b) indicate the order in which the drips fall after the fire starts, corresponding to drip number N in (c). White scale bars: 2 cm in (a) and 5 mm in (b).

maximum flame size per drip increases with time due to the gradually increasing T_s. Towards the end of this stage, the accumulation of the droplets on the substrate is nearly burned or evaporated ($t_3 = 22.155$ s in Fig. 3b). Although the fire remains relatively stable at this stage, the top of the flame gradually turns yellow due to the intensifying combustion (as seen at 20.1 s in Fig. 3a, indicating inadequate combustion).

Stage 3 is featured by the motion of the burning droplet. The droplet is no longer stationary but starts to migrate from the center (impact point) towards the edge of the substrate. At this moment, the flame becomes very small (observed at 23.4 s in Fig. 3a). Due to the limited size of the substrate (35 mm in side length), the newly arrived drips can be easily ignited by the burning droplets previously transported towards the edge, resulting in multiple burning droplets on the substrate (see at 28.2 s and 52.0 s in Fig. 3a). Monitoring the substrate temperature reveals that the motion of the burning droplet is induced by the uneven temperature distribution across the substrate (represented by the shaded band around the temperature curve in Fig. 3c). In other words, the substrate temperature at the center is higher than that at the edge, primarily due to the heat transfer from the high-temperature flame to the substrate. This directed motion of the burning droplet from the hot zone (center) to the cold zone (edge) is known as thermocapillary effect [19, 20]. It should be noted that the evaporation of the burning droplets are at contact boiling [21,22] because the substrate temperature T_s exceeds the boiling point of the liquid (for ethanol, $T_{boil} = 78$ °C). Simultaneously, the movement of the burning droplet towards the colder region in turn affects the uneven temperature distribution on the substrate, gradually weakening the thermocapillary effect. This can be observed by the decreasing shadow around the temperature curve at $t_3 \sim t_4$ in Fig. 3c. Additionally, the flame size at later times is significantly larger than during stage 2 ($t_2 \sim t_3$ in Fig. 3c). The higher overall temperature of the substrate leads to rapid evaporation of the burning droplet, extinguishing the fire before the next drip arrives (as depicted in Fig. 3b, the burning droplet has completely evaporated at $t_4 = 65.190$ s, while the next drip reaches the substrate at 65.299 s). Just before dying out (at 64.3 s in Fig. 3a), the bright yellow color of the flame indicates strong and inadequate burning, along with a high evaporation rate of the droplet.

In the above experiments, we consider the effect of the number N_0 of starting droplets on fire self-extinguishing. As shown in Fig. S1, we find that its effect is negligible within a range of $N_0 = 3 \sim 9$ due to the similar substrate temperature changes. Additionally, we investigate the influence of the Weber number We (impact velocity v_0) and the initial substrate temperature T_0 ($< T_{boil}$) on fire self-extinguishing in Fig. S2. We observe that the burning time t_b of the fire increases as We increases or T_0 decreases. The reason for this is twofold: firstly, an increased We creates droplet splashing and reduces the mass of the burning liquid on the substrate, thereby slowing down the substrate heating rate and prolonging the time to reach the self-extinguishing temperature. Secondly, a lower T_0 directly weakens the droplet evaporation, resulting in a longer time for the burning droplet to self-extinguish.

3.2. Burning regimes

The above results are discussed based on constant drip mass m_0 and frequency f. However, since self-extinguishing is caused by the rapid evaporation of the burning droplet on the heated substrate before the arrival of the next drip, it is very necessary to study the influence of m_0 and f on the burning time and regime of dripping fire. In Fig. 4a and b, the drip frequency f is firstly changed to observe the burning time t_b of the fire and the final temperature T_{final} of the substrate in an ethanol dripping fire. With the increasing f, the burning time t_b is found to increase gradually and eventually to be out of control ($f > 2.3$ Hz, burning for more than 10 min, not represented by symbols) in Fig. 4a. Correspondingly, the final temperature T_{final} of the substrate first increases and then remains stable in Fig. 4b. It should be noted that a jump in t_b and T_{final} is observed at $f = 0.4 \sim 0.5$ Hz, where T_{final} jumps from 60 °C to 91 °C, and t_b jumps from 13 to 51 s. This jump is attributed to the thermocapillary effect of burning droplets, which occurs when T_s approaches 73 °C (close to the boiling point of ethanol, see Fig. S3a and b). Although the overall temperature of the substrate is rising, the transport of burning droplets from the hot zone (center) to the cold zone (edge) prolongs the fire's lifetime. Therefore, according to the variation of t_b and T_{final}, we can divide the ethanol dripping fire into three different burning regimes in Fig. 4a and b: non-igniting (gray region), self-extinguishing (orange region), and non-extinguishing (blue region). In a non-igniting regime, the slight increase in t_b (1.3 ~ 6.8 s) and T_{final} (25.9 ~ 47.9 °C) is attributed to the burning of the kindling liquid film, which is extinguished before the first drip arrives. In a self-extinguishing

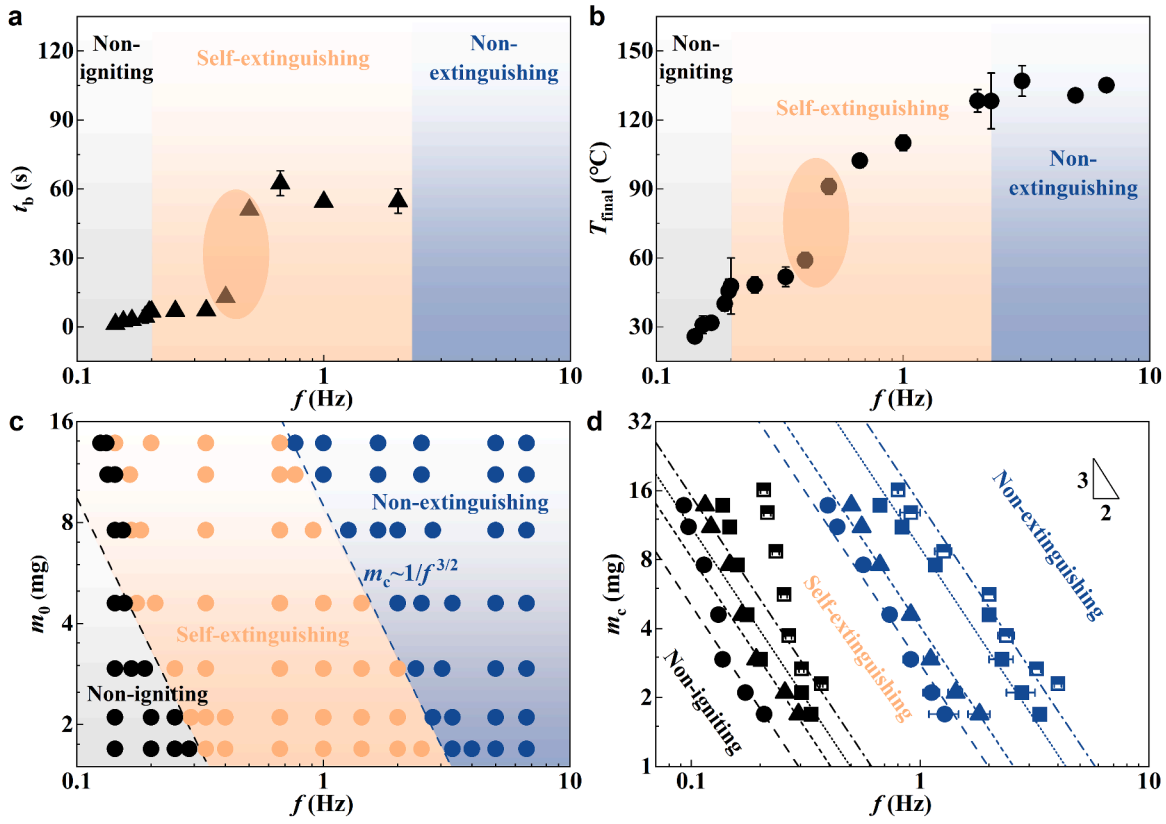

Fig. 4. Phase diagram. (a-b) The burning time t_b of the fire and the final temperature T_{final} of the substrate as a function of drip frequency f ($m_0 = 2.9$ mg, $We = 305$). The gray, orange, and blue regions represent the non-igniting, self-extinguishing, and non-extinguishing regimes, respectively. (c) Burning regimes of ethanol dripping fire on a smooth silicon substrate controlled by m_0 and f. (d) The critical drip mass m_c as a function of f in different liquid and substrate types at the boundaries of the burning regime. The substrates are silicon (square symbol), sapphire (triangle symbol), and quartz (circular symbol), and the liquids are ethanol (solid symbols, $We = 254 \sim 514$) and methanol (semi-solid symbols, $We = 277 \sim 531$). Black symbols indicate the occurrence of self-extinguishing or non-igniting regimes, while blue symbols indicate the occurrence of self-extinguishing or non-extinguishing regimes. Error bars in (a-d) are obtained from the standard deviation calculated by ten repeated experiments. The boundaries of the burning regime in (c and d) satisfy the scaling $m_c \sim 1/f^{3/2}$.

regime, the number of drips that can be ignited increases with the drip frequency f, so that t_b and T_{final} vary in the range of 7.0 ~ 62.5 s and 48.3 ~ 128.4 °C, respectively. However, as f is further increased, the fire enters a non-extinguishing regime. This is because the high f ensures that the fire keeps being replenished by the ethanol drips, and eventually T_{final} reaches a dynamic equilibrium (~ 130 °C), so we can observe the fire burning for more than 10 min.

The mass m_0 of the drip is also another important factor affecting the burning regime. In Fig. 4c, we show a phase diagram of burning regimes dependent on m_0 and f for ethanol dripping fire on a smooth silicon substrate, where the two boundaries (black and blue dashed lines) of the burning regime are found to scale as $m_c \sim 1/f^{3/2}$ (m_c is the critical mass of the drip). This scaling is confirmed when we repeat the same experiment with different liquids (methanol) and substrates (silicon, sapphire, and quartz) in Fig. 4d. We find a good agreement between the scaling and the experimental results, except for some deviations at the boundary between the non-igniting and self-extinguishing regimes (black dashed lines in Fig. 4c and d). This deviation is due to the heat transfer from the high-temperature flame to the substrate increasing with the mass of the drip, which in turn causes the evaporation of the droplet on the substrate to be further enhanced (see Fig. S4a-b, T_{final} at the regime boundary can reach up to 60 °C when the mass m_0 of the drip is 13.8 mg). To keep on the fire, the drip frequency f (black symbols in Fig. 4d) has to be larger in experiments than predicted by the scaling to enter the self-extinguishing from the non-igniting. T_{final} is also found to be dominated by the liquid properties and is not strongly affected by the drip frequency f and the substrate material at the boundary between the self-extinguishing and non-extinguishing regimes in Fig. S4a-b. Specifically, T_{final} for methanol dripping fire is approximately 86 °C, while that for ethanol dripping fire is about 127 °C. This demonstrates that the burning regime of dripping fire depends on the drip mass and frequency, and the boundaries of the burning regime are affected by the type of liquid and substrate.

3.3. Mechanism and model of a self-extinguishing regime

As mentioned previously, the interaction between continuous flammable drips and the impacted substrate affects the burning regime of the fire, in which the thermal state of the substrate plays a crucial role in triggering the self-extinguishing fire. To provide a more comprehensive understanding of the burning regime and time of the dripping fire, a schematic diagram illustrating the evaporation of a burning droplet on a hot substrate is depicted in Fig. 5a. Two key thermal parameters, q_l (J/s) and q_s (W) are defined, namely the heat release rate of a burning droplet and the heat transfer power of the substrate. They can be expressed as $q_l \sim m_0 \Delta H f$ and

$$q_s \sim \frac{D_0^2 f_s \lambda_{sl} \Delta T}{\left(3\tan\frac{\theta}{2} + \tan^3\frac{\theta}{2}\right)^{2/3}},$$

respectively, where ΔH is the heat of combustion, θ is the static solid-liquid contact angle, f_s is the solid area fraction, λ_{sl} is the interfacial heat transfer coefficient, and ΔT is the temperature difference between the substrate and the droplet surface. The detailed derivation of q_l and q_s can be found in the Supplementary Material. In a dripping fire, the parameter q_l dominates the final fate (burning regime) of the fire,

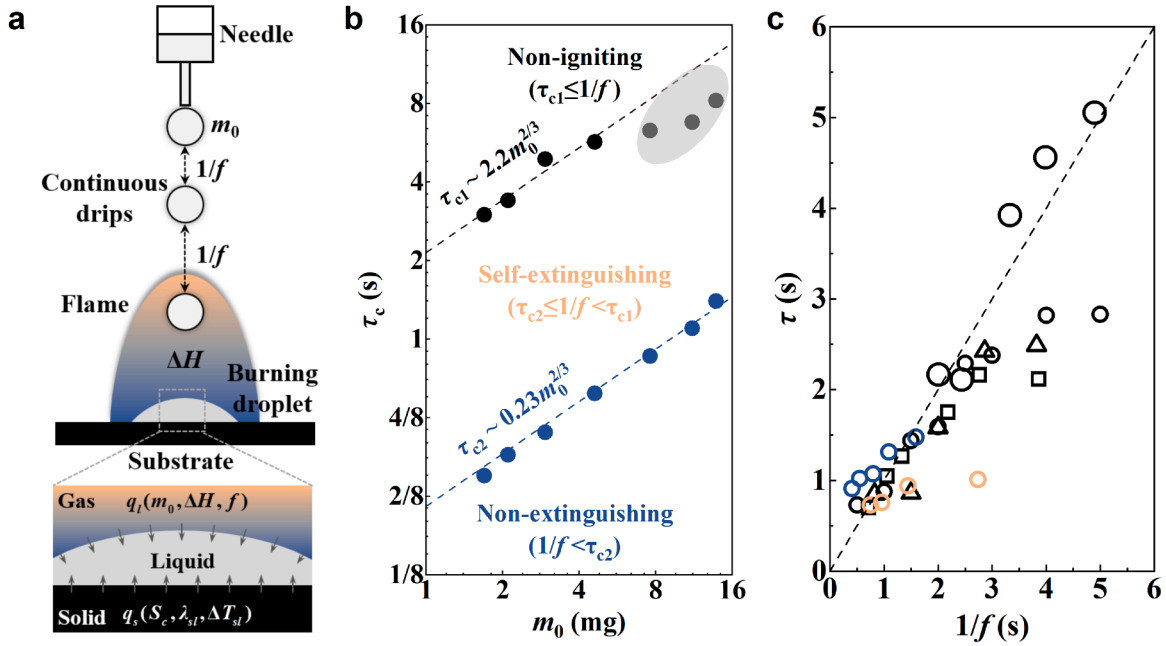

Fig. 5. The influence mechanism of dripping fires and the validation of a self-extinguishing predictive model. (a) Schematic diagram of the thermal effects of q_l and q_s on the dripping fire. (b) The lifetime τ_c of a burning liquid on a smooth silicon substrate as a function of m_0 at the boundaries of the burning regime. They all adhere to $\tau_c \sim m_0^{2/3}$ except for the gray region due to the influence of substrate temperature. (c) The comparison of a predictive lifetime τ with the experimental drip time $1/f$ in different self-extinguishing dripping fires. Three liquids (ethanol (black symbol), methanol (blue symbol), and isooctane (orange symbol)) and three substrate materials (silicon (round symbol), sapphire (triangle symbol), and quartz (square symbol)) are tested. The large symbols represent the case where $m_0 = 11.1$ mg ($We = 477$), while the small symbols represent the case where $m_0 = 2.9$ mg ($We = 305$).

whether it be non-igniting, self-extinguishing, or non-extinguishing. The parameter q_s affects the rate at which a burning droplet evaporates on a hot substrate, ultimately influencing how quickly the fire is extinguished. As q_l decreases, the possibility of the next drip being ignited reduces, making it increasingly difficult to sustain the fire. This explanation aligns with the experimental results depicted in Fig. 4, where the ethanol dripping fire transitions from non-extinguishing to non-igniting as m_0 and f decrease. Additionally, the methanol dripping fire, which has a lower ΔH, exhibits a larger non-igniting region when compared to ethanol. Conversely, as q_s increases, the droplet evaporation is enhanced, resulting in a shortened t_b. This leads to faster extinguishing, as seen in the experimental results in Fig. 4d, where an increase in thermal conductivity λ_s from quartz to silicon expands the non-igniting region. In reality, whether a fire is self-extinguishing or not depends on the time it takes for the next drip to reach the substrate surface relative to the lifetime of the burning liquid on the substrate. In Fig. 5b, the transitions between non-igniting, self-extinguishing, and non-extinguishing regimes can be characterized by two critical times τ_{c1} and τ_{c2}, where τ_{c1} represents the burning time of the kindling liquid film and τ_{c2} corresponds to the burning time of the last drip before the fire self-extinguishes. If the first drip fails to reach the substrate surface before the kindling liquid film burns out (i.e. $\tau_{c1} \leq 1/f$), the fire is non-igniting. Conversely, if the droplet is still burning on the substrate when the next drip reaches the surface (i.e. $\tau_{c2} > 1/f$), the fire is non-extinguishing. In cases where $\tau_{c2} \leq 1/f < \tau_{c1}$, the fire is self-extinguishing.

Given the complexity of continuous impact and droplet combustion in a dripping fire, accurately predicting the self-extinguishing behavior for specific drip parameters m_0 and f is challenging. However, it is crucial to quantitatively analyze the critical conditions for fire self-extinction. To address this, a simplified physical model of a burning droplet evaporating on a hot substrate is developed and illustrated in Fig. S5a. In this model, there are two primary heat sources: high-temperature flames (involving gas-liquid heat transfer with flame temperature typically exceeding 1000 °C) and hot substrates (involving solid-liquid heat transfer through contact boiling). These heat sources drive the evaporation of the burning droplet. To simplify the analysis, we consider the heat contributions separately and decouple the mixed evaporation mode into two parts: the evaporation of an unburned sessile droplet and the evaporation of a hanging burning droplet (represented by the simplified schematic diagram in Fig. S5b-c). Next, we derive the droplet mass loss rate for each part and establish an expression $\tau = D_0^2/K^*$ for the lifetime of a burning droplet on a hot substrate, which is also known as D^2 law [23–25]. In this law, K^* is a burning constant that depends on various factors such as droplet combustion characteristics, substrate thermal conductivity and wetting characteristics, and environmental conditions. The detailed derivation process for K^* is provided in the Supplementary Material. Since the lifetime of a burning droplet satisfies $\tau \sim D_0^2$, we have $\tau \sim m_0^{2/3}$. At the regime boundary, it follows $\tau \sim m_c^{2/3}$ and $\tau = 1/f$, which finally yields $m_c \sim 1/f^{3/2}$. The results of these derivations agree with the experimental findings presented in Fig. 4c, d and 5b. Utilizing the D^2 law, Fig. 5c presents the predicted and experimental values of the lifetime of the last burning droplet in self-extinguishing dripping fires for different liquid types and substrate materials. It is worth noting that some of the predicted values τ deviate from the experimental results $1/f$, which can be attributed to the uncertainty in calculating K^*. The uncertainty stems from the dynamic variations of physical parameters (such as θ and T_s) during droplet evaporation, while their average or transient values are used in the calculation of K^*. Furthermore, due to the intricate nature of droplet combustion and heat transfer, certain physically challenging parameters (such as heat parameters associated with flame temperature and vapor zone) are obtained from previous studies or referenced from physical chemistry handbooks [26–28]. As a consequence, deviations between theoretical and experimental values are inevitable. Nevertheless, by extensively testing a wide range of liquid types and substrate materials, along with varying m_0 and f, we observe that the predicted values τ from our theoretical model are of the same order of magnitude (O(0.1) ~ O(1)) as $1/f$. This suggests the reliability of our model in predicting the self-extinguishing behavior of a dripping fire.

3.4. Tunable dripping fire on different impacted substrates

We design a range of substrates, including microtextured surfaces (such as micropore, micropillar and microgroove) and rough surfaces (0.1 μm < *Ra* < 1 μm, including silicon, sapphire and quartz) to manipulate surface structures and thermal properties of the substrate, thereby altering thermocapillary motion and evaporation behavior of burning droplets, and ultimately regulating their lifetime to achieve tunable self-extinguishing of dripping fires.

As depicted in Fig. 6a–f, we compare the duration t_b of the fire on six different substrates with identical drip parameters (ethanol, $m_0 = 2.9$ mg, $We = 305$, $f = 0.67$ Hz). The results demonstrate that t_b is significantly shorter on microtextured surfaces (indicated by only the first two burning stages in Fig. 6a–c, flame size presented in Fig. S6a-b), but longer on rough surfaces (characterized by three burning stages in Fig. 6d–f, flame size shown in Fig. S6c-d). This discrepancy arises from the fact that the microtextures on the substrate impede the thermocapillary motion of the burning droplets due to the fixed three-phase contact line [29], whereas on the rough, the moving burning droplets are still observable. Furthermore, schematic diagrams presented in Fig. 6a–f clearly demonstrate that t_b on microtextured surfaces is influenced by the contact angle θ and the solid area fraction f_s, while on rough surfaces, it is primarily dominated by the thermal conductivity λ_s. Specifically, for the three microtextures, it can be observed that the duration of each burning stage on microporous surfaces ($t_{b1} = 16.4$ s and $t_{b2} = 24.6$ s in Fig. 6a) is longer compared to that on micropillared surfaces ($t_{b1} = 8.7$ s and $t_{b2} = 13.3$ s in Fig. 6b). This can be attributed to the slowing down of droplet evaporation with the increase of θ [30] ($\theta = 50.1^\circ$ for micropore and $\theta = 17.4^\circ$ for micropillar, see Movie S2). Additionally, it is observed that the duration of each burning stage on microgrooved surfaces ($t_{b1} = 4.9$ s and $t_{b2} = 14.3$ s in Fig. 6c) is shorter than that on micropillared surfaces. Apart from the effect of θ, this is mainly owing to the acceleration of droplet evaporation with the increase of f_s [31] ($f_s = 5$ for microgroove and $f_s = \pi+1$ for micropillar, see Movie S3). The influence of θ and f_s is further confirmed by the time-dependent S_c [32,33] on the microtextured surface in Fig. S7a. Finally, microgrooved surfaces with smaller θ and larger f_s exhibit the fastest extinguishing of the dripping fire among all the microtextured surfaces ($t_b = 19.2$ s in Fig. 6c). In contrast, for the three materials tested, the duration of each burning stage on silicon surfaces ($t_{b1} = 11.1$ s, $t_{b2} = 10.9$ s and $t_{b3} = 26.6$ s in Fig. 6d) is significantly shorter than that on sapphire surfaces ($t_{b1} = 12.6$ s, $t_{b2} = 24.6$ s and $t_{b3} = 94.3$ s in Fig. 6e). This is due to the acceleration of droplet evaporation with increasing thermal conductivity λ_s [34,35]. However, we have also found that when λ_s is poor (such as in the case of quartz with $\lambda_s = 1.39$ W·m^{-1}·K^{-1}), the duration of each burning stage is also short ($t_{b1} = 7.8$ s, $t_{b2} = 8.3$ s and $t_{b3} = 26.9$ s in Fig. 6f). Based on the burning process (see Movie S4) and the measured substrate temperature (Fig. S7d), it can be seen that the

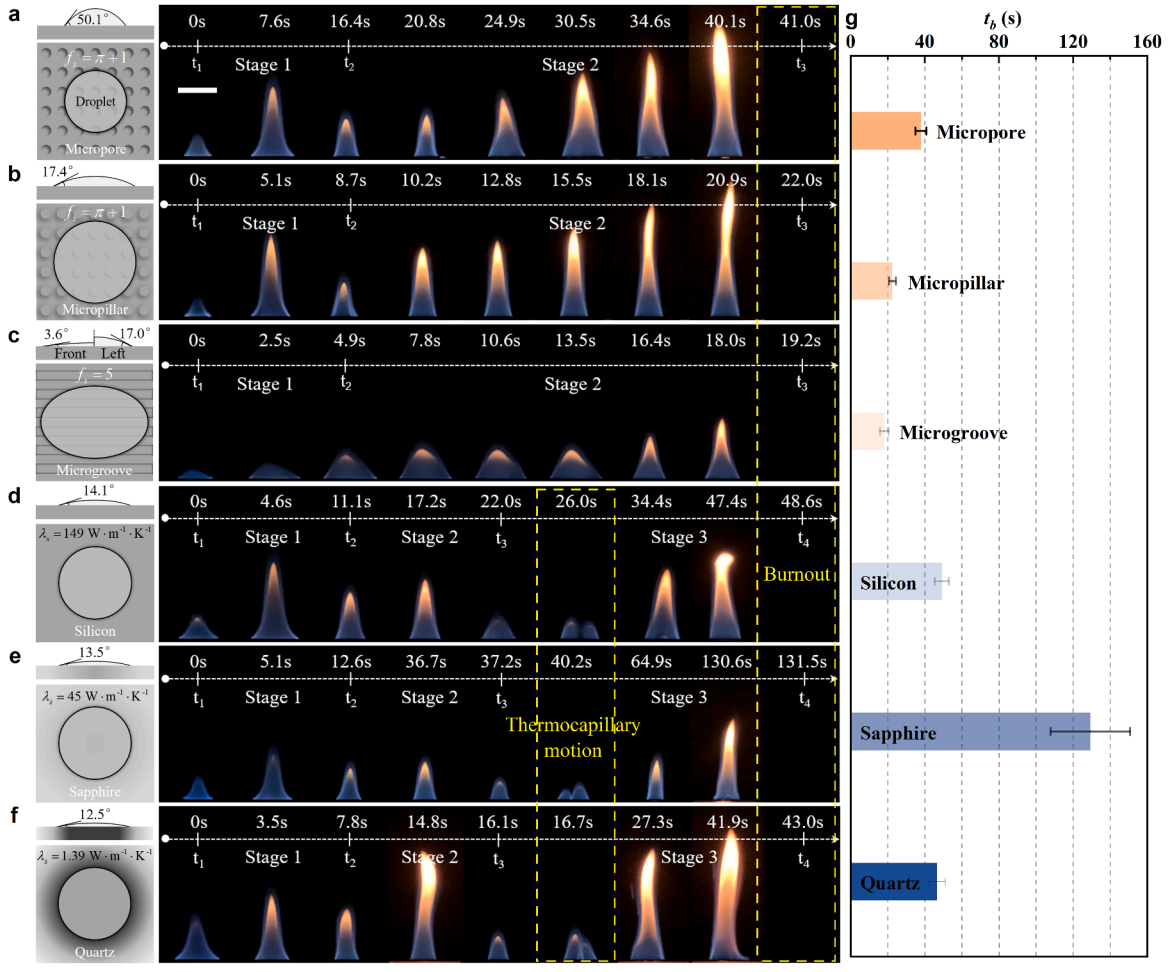

Fig. 6. Tunable dripping fire on different impacted substrates. (a–f) Self-extinguishing ethanol dripping fires on various substrates ($m_0 = 2.9$ mg, $We = 305$, $f = 0.67$ Hz). Microtextured surface: (a) micropore, (b) micropillar, (c) microgroove. Rough surface: (d) silicon, (e) sapphire, (f) quartz. Each figure includes a diagram of the side-view wetting state and the top-view evaporation shape of an ethanol droplet on the corresponding substrate, and flame snapshots before the fire self-extinguishes. The substrate surfaces are color-coded, with darker shades indicating higher temperatures. The white scale bar is 2 cm. (g) A comparison of the fire duration t_b on different substrates. The error bar is the standard deviation of ten sets of experiments.

temperature distribution on the quartz surface is highly non-uniform. Surprisingly, local temperatures on the quartz surface can even be higher than those on the silicon surface (λ_s = 149 W·m^{-1}·K^{-1}). As a result, the burning droplet in the hot zone experiences a high evaporation rate [36] before it moves towards the cold zone. Consequently, a burning droplet on a poorly heat-conducting quartz substrate can boil as rapidly as on a well heat-conducting silicon substrate, leading to the suppression of thermocapillary motion. In contrast, droplet evaporation occurs at a slower rate on a moderately heated sapphire substrate (λ_s = 45 W·m^{-1}·K^{-1}). The inhomogeneous temperature distribution on sapphire surfaces induces a persistent thermocapillary effect (see Movie S4), thus significantly prolonging the duration of the fire (t_b = 131.5 s in Fig. 6e). Finally, we summarize the fire durations t_b on different substrate surfaces in Fig. 6g. The fire on the microgrooved surface exhibits the shortest duration (t_b = 18.1 ± 2.4 s), while that on the sapphire surface has the longest duration(t_b = 129.3 ± 21.4 s). The fire duration on the sapphire surface is over 7 times longer than that on the microgrooved surface in a self-extinguishing fire.

4. Conclusion

In this study, we focus on understanding the behavior of dripping fires and how they self-extinguish. Dripping fires occur when a flammable liquid, such as oil or gasoline, drops onto a substrate and ignites. We investigate how the overall temperature and temperature distribution of the substrate affect the self-extinguishing process. We find that droplet evaporation, which plays a crucial role in the burning process, is influenced by both the overall temperature and temperature heterogeneity of the substrate. As the overall temperature of the substrate increases, droplet evaporation also increases. However, when there is a non-uniform temperature distribution on the substrate, droplet evaporation decreases. This is because the temperature difference induces thermocapillary motion, causing the burning droplet to move from the hot zone to the cold zone on the substrate. Furthermore, we analyze the effect of drip parameters, such as the mass and the frequency of the drip, on the behavior of the fire. Based on the experimental results, we categorize the phase diagram into three burning regimes: non-igniting, self-extinguishing, and non-extinguishing. We find that the boundaries of these burning regimes scale as $m_c \sim 1/f^{3/2}$. This scaling relationship holds for different liquids and substrates. To predict the self-extinguishing behavior of a dripping fire, we develop a physical model for the evaporation of a burning droplet on a hot substrate, which aligns well with our experimental findings. Additionally, we design various substrates with different surface structures and thermal properties to regulate the burning time of dripping fires. For example, we find that sapphire substrates can extend the burning time to over 120 s, while microgrooved substrates can shorten it to under 20 s. Overall, our study provides valuable insights into controlling the burning time caused by flammable drips in building and industrial settings. The findings can be applied to develop effective fire prevention and suppression strategies to enhance safety in these environments.

CRediT authorship contribution statement

Xujun Fan: Writing – review & editing, Writing – original draft, Investigation, Formal analysis. **Fangye Lin:** Writing – review & editing, Formal analysis. **Stéphane Dorbolo:** Writing – review & editing, Supervision. **Wei Wang:** Methodology. **Jun Zou:** Supervision, Funding acquisition.

Declaration of competing interest

The authors declare that they have no known competing financial interests or personal relationships that could have appeared to influence the work reported in this paper.

Data availability

Data will be made available on request.

Acknowledgments

This work was supported by the Zhejiang Provincial Natural Science Foundation of China (LD22E050002). S. Dorbolo thanks F.R.S.-FNRS for financial support as a Senior Research Associate.

Supplementary materials

Supplementary material associated with this article can be found, in the online version, at doi:10.1016/j.ijheatmasstransfer.2024.125262.

References

[1] M. Calvin, New sources for fuel and materials, Science 219 (1983) 24–26.
[2] X. Ma, R. Tu, W. An, L. Xu, S. Luo, J. Wang, F. Tang, Experimental study of interlayer effect induced by building facade curtain wall on downward flame spread behavior of polyurethane, Appl. Therm. Eng. 167 (2020) 114694.
[3] J.I. Chang, C.C. Lin, A study of storage tank accidents, J. Loss Prev. Process Ind. 19 (2006) 51–59.
[4] H. He, Q. Zhang, R. Tu, L. Zhao, J. Liu, Y. Zhang, Molten thermoplastic dripping behavior induced by flame spread over wire insulation under overload currents, J. Hazard. Mater. 320 (2016) 628–634.
[5] X. Huang, Critical drip size and blue flame shedding of dripping ignition in fire, Sci. Rep. 8 (2018) 16528.
[6] P. Sun, S. Lin, X. Huang, Ignition of thin fuel by thermoplastic drips: an experimental study for the dripping ignition theory, Fire Saf. J. 115 (2020) 103006.
[7] X. Wang, X. Cheng, L. Li, S. Lo, H. Zhang, Effect of ignition condition on typical polymer's melt flow flammability, J. Hazard. Mater. 190 (2011) 766–771.
[8] P. Sun, S. Lin, X. Huang, Ignition of thin fuel by thermoplastic drips: an experimental study for the dripping ignition theory, Fire Saf. J. 115 (2020) 103010.
[9] Q. Xie, R. Tu, N. Wang, X. Ma, X. Jiang, Experimental study on flowing burning behaviors of a pool fire with dripping of melted thermoplastics, J. Hazard. Mater. 267 (2014) 48–54.
[10] Y. Kim, A. Hossain, Y. Nakamura, Numerical modeling of melting and dripping process of polymeric material subjected to moving heat flux: prediction of drop time, Proc. Combust. Inst. 35 (2015) 2555–2562.
[11] H. He, Q. Zhang, R. Tu, L. Zhao, J. Liu, Y. Zhang, Molten thermoplastic dripping behavior induced by flame spread over wire insulation under overload currents, J. Hazard Mater. 320 (2016) 628–634.
[12] F. Carosio, A.P. Di, J. Alongi, A. Fina, G. Saracco, Controlling the melt dripping of polyester fabrics by tuning the ionic strength of polyhedral oligomeric silsesquioxane and sodium montmorillonite coatings assembled through layer by layer, J. Colloid Interface Sci. 510 (2018) 142.
[13] Q. Guan, X. Lu, Y. Chen, H. Zhang, Y. Zheng, R.E. Neisiany, Z. You, High-performance liquid crystalline polymer for intrinsic fire-resistant and flexible triboelectric nanogenerators, Adv. Mater. 34 (2022) 2204543.
[14] T. Wu, F. Yang, J. Tao, H. Zhao, C. Yu, W. Rao, Design of p-decorated poss towards flame-retardant, mechanically-strong, tough and transparent epoxy resins, J. Colloid Interface Sci. 640 (2023) 864–876.
[15] C. Xiong, Y. Liu, C. Xu, X. Huang, Extinguishing the dripping flame by acoustic wave, Fire Saf. J. 120 (2021) 103109.
[16] C. Xiong, Y. Liu, H. Fan, X. Huang, Y. Nakamura, Fluctuation and extinction of laminar diffusion flame induced by external acoustic wave and source, Sci. Rep. 11 (2021) 14402.
[17] X. Fan, C. Wang, F. Guo, Experimental study of flame expansion induced by water droplet impact on the burning cooking oil, Fuel 270 (2020) 117497.
[18] M. Xu, J. Zhang, R. Chen, S. Lu, Single droplet with or without additives impacting on high-temperature burning liquid pool, Int. J. Heat Mass Transf. 139 (2019) 77–86.
[19] Q. Dai, M.M. Khonsari, C. Shen, W. Huang, X. Wang, Thermocapillary migration of liquid droplets induced by a unidirectional thermal gradient, Langmuir 32 (2016) 7485–7492.
[20] Q. Dai, S. Chen, W. Huang, X. Wang, S. Hardt, On the thermocapillary migration between parallel plates, Int. J. Heat Mass Transf. 182 (2022) 121962.
[21] T. Tran, H.J. Staat, A. Prosperetti, C. Sun, D. Lohse, Drop impact on superheated surfaces, Phys. Rev. Lett. 108 (2012) 36101.
[22] M. Khavari, T. Tran, Time-dependent measurements of length and area of the contact line in contact-boiling regime, J. Fluid Mech. 926 (2021) R3.
[23] J.C. Maxwell, The Scientific Papers of James Clerk Maxwell, vol. 2, Cambrige University Press, 1890.
[24] M.A. Saxton, J.P. Whiteley, D. Vella, J.M. Oliver, On thin evaporating drops: when is the d2-law valid? J. Fluid Mech. 792 (2016) 134–167.

[25] J. Shaikh, A. Sharma, R. Bhardwaj, On sharp-interface level-set method for heat and/or mass transfer induced stefan problem, Int. J. Heat Mass Transf. 96 (2016) 458–473.
[26] W.M. Haynes, D.R. Lide, T.J. Bruno, CRC Handbook of Chemistry and Physics, 97th ed., CRC Press, Boca Raton, 2016.
[27] T.L. Bergman, A.S. Lavine, F.P. Incropera, D.P. Dewitt, Fundamentals of Heat and Mass Transfer, 7th ed., John Wiley and Sons, 2011.
[28] F.A. Kulacki, Handbook of Thermal Science and Engineering, 1st ed., Springer, 2011.
[29] Q. Dai, W. Huang, X. Wang, A surface texture design to obstruct the liquid migration induced by omnidirectional thermal gradients, Langmuir 31 (2015) 10154–10160.
[30] C. Bourgks-Monnier, M.E.R. Shanahan, Influence of evaporation on contact angle, Langmuir 11 (1995) 2820–2829.
[31] J.H. Moon, M. Cho, S.H. Lee, Dynamic wetting and heat transfer characteristics of a liquid droplet impinging on heated textured surfaces, Int. J. Heat Mass Transf. 97 (2016) 308–317.
[32] J. Li, L. Shan, B. Ma, X. Jiang, A. Solomon, M. Iyengar, J. Padilla, D. Agonafer, Investigation of the confinement effect on the evaporation behavior of a droplet pinned on a micropillar structure, J. Colloid Interface Sci. 555 (2019) 583–594.
[33] K. Chen, R. Xu, P. Jiang, Evaporation enhancement of microscale droplet impact on micro/nanostructured surfaces, Langmuir 36 (2020) 12230–12236.
[34] S. David, K. Sefiane, L. Tadrist, Experimental investigation of the effect of thermal properties of the substrate in the wetting and evaporation of sessile drops, Colloids Surf. A Physicochem. Eng. Asp. 298 (2007) 108–114.
[35] B. Sobac, D. Brutin, Thermal effects of the substrate on water droplet evaporation, Phys. Rev. E 86 (2012) 21602.
[36] C. Hsu, T. Su, C. Wu, L. Kuo, P. Chen, Influence of surface temperature and wettability on droplet evaporation, Appl. Phys. Lett. 106 (2015) 141602.